# Quad-LED OTFS Modulation in Indoor Visible Light Communication Systems

Sujata Sinha and A. Chockalingam
Department of ECE, Indian Institute of Science, Bangalore 560012

GLOBECOM 2021 - 2021 IEEE Global Communications Conference | 978-1-7281-8104-2/21/$31.00 ©2021 IEEE | DOI: 10.1109/GLOBECOM46510.2021.9685670

***Abstract*—In this paper, we investigate orthogonal time frequency space (OTFS) modulation in multi-LED indoor visible light wireless communications. Specifically, we propose two quad-LED OTFS schemes, namely, 1) quad-LED complex modulation OTFS (QCM-OTFS), and 2) spatial modulation dual-LED complex modulation OTFS (SM-DCM-OTFS). The proposed QCM-OTFS scheme sends the magnitudes of real and imaginary parts of complex signals through intensity modulation (IM) and their sign information through spatial indexing of LEDs. The proposed SM-DCM-OTFS scheme sends the magnitude and phase of complex signals (polar representation) through a pair of LEDs and frame indexing across two pairs of LEDs. The proposed schemes do not require Hermitian symmetry and DC bias operations to obtain real positive valued signals suited for IM of LEDs. We obtain upper bounds on the bit error rate (BER) performance of the proposed schemes, which are tight at high signal-to-noise ratios (SNR). Compared to the QCM-OFDM and SM-DCM-OFDM schemes known in the literature, the proposed schemes achieve significantly better BER performance. We also analyze the spatial distribution of the SNR gain in the proposed QCM-OTFS/SM-DCM-OTFS schemes compared to QCM-OFDM/SM-DCM-OFDM schemes using the ratio of minimum distance of normalized received signal sets as a metric.**

***Keywords:*** *Visible light communication, OTFS modulation, multi-LED transmission, quad-LED OFDM/OTFS.*

## I. Introduction

Visible light communication (VLC) technology is emerging as an attractive technology for wireless communications in indoor and vehicular environments [1],[2]. Modulation schemes and signal processing techniques for VLC [3], such as multiple-input multiple-output (MIMO) modulation schemes [4],[5] and orthogonal frequency division multiplexing (OFDM) techniques [6]-[9], have been widely investigated in the VLC literature. OFDM techniques in VLC systems employ Hermitian symmetry (which causes rate loss) or DC bias to convert complex information symbols into real, positive-valued signals suited for intensity modulation of LEDs. Multi-LED techniques for OFDM transmission without Hermitian symmetry or DC-bias that employ spatial indexing of LEDs have been reported. These include quad-LED complex modulation OFDM (QCM-OFDM) and dual-LED complex modulation OFDM (DCM-OFDM) [10], [11].

Recently, in the RF communication domain, a new modulation scheme called orthogonal time frequency space (OTFS) modulation has been shown to achieve significantly better performance compared to OFDM, particularly in high-Doppler channels [12]-[15]. It has been further shown that OTFS performs very well in static multipath channels as well [16]. Motivated by this, in this paper, we investigate OTFS modulation in indoor VLC (where the channel gains are almost static) and compare its performance with that of OFDM.

OTFS is a two-dimensional (2D) modulation scheme, where $MN$ information symbols are multiplexed in the delay-Doppler (DD) domain using $M$ Doppler bins and $N$ delay bins. These symbols in the DD domain are mapped to time domain using 2D transformations. Recently, in [17], OTFS has been studied for optical wireless communication (OWC) by considering a single-LED DC-biased optical (DCO) scheme along with OTFS. This study has revealed that DCO-OTFS can perform significantly better than DCO-OFDM in OWC systems. Carrying this line of research forward, in this paper, we propose two promising quad-LED VLC transmitter architectures employing OTFS. The first architecture is a quad-LED complex modulation OTFS (QCM-OTFS) architecture where four LEDs are used to send the magnitudes of real and imaginary parts of complex signals through intensity modulation (IM) of LEDs and the sign information is conveyed through spatial indexing of LEDs. The second architecture is a spatial modulation dual-LED complex modulation OTFS (SM-DCM-OTFS) architecture, where the magnitude and phase of complex signals are sent through a pair of LEDs and an additional bit is conveyed using frame indexing across two pairs of LEDs. Both the architectures eliminate the need for Hermitian symmetry and DC-bias. Our new contributions in this paper can be summarized as follows.

- We obtain analytical upper bounds on the BER performance of the proposed QCM-OTFS and SM-DCM-OTFS schemes, which are found to be tight at high signal-to-noise ratios (SNR).
- Our analytical and simulation results show that the proposed QCM-OTFS and SM-DCM-OTFS schemes achieve better performance, respectively, compared to QCM-OFDM and SM-DCM-OFDM schemes known in the VLC literature.
- Using the ratio of the minimum distance of different normalized received signal sets as a metric, we quantify the spatial distribution of the SNR gain in the proposed QCM-OTFS/SM-DCM-OTFS schemes compared to the QCM-OFDM/SM-DCM-OFDM schemes.

This work was supported in part by J. C. Bose National Fellowship, Department of Science and Technology, Government of India, and the Centre for Networked Intelligence (a Cisco CSR initiative) of the Indian Institute of Science, Bangalore.

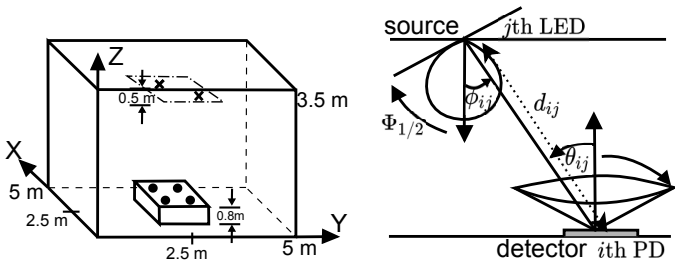


Fig. 1: Indoor VLC system setup. A cross represents an LED and a dot represents a PD.

## II. Indoor VLC system model

Consider an indoor MIMO VLC system consisting of $N_t$ transmit LEDs and $N_r$ receive PDs in a room of dimension 5m $\times$ 5m $\times$ 3.5m as shown in Fig. 1. Each LED is either OFF or emits some intensity whose magnitude is based on the complex modulated signal sent in each channel use. The proposed QCM-OTFS and SM-DCM-OTFS schemes (presented in the next section) are block transmission schemes that employ multiple channel uses (say, $Q$ channel uses) for transmission. Let $\mathbf{X}$ denote the $N_t \times Q$ transmit matrix, given by

$$\mathbf{X} = \begin{bmatrix} x[1,1] & x[1,2] & \cdots & x[1,Q] \\ x[2,1] & x[2,2] & \cdots & x[2,Q] \\ \vdots & \vdots & \ddots & \vdots \\ x[N_t,1] & x[N_t,2] & \cdots & x[N_t,Q] \end{bmatrix},$$

where $x_j$ denotes the intensity of light transmitted by the $j$th LED. We assume that the LEDs have Lambertian radiation pattern. We consider a static channel with line-of-sight (LOS) paths between the LEDs and the PDs. The channel matrix $\mathbf{H}$ is of order $N_r \times N_t$, whose $(i,j)$th element $h_{ij}$ is the LOS channel gain between the $j$th LED and $i$th PD given by [1]

$$h_{ij}^{\text{LOS}} = \frac{n+1}{2\pi} \cos^n \phi_{ij} \cos\theta_{ij} \frac{A}{d_{ij}^2} \operatorname{rect}\left(\frac{\theta_{ij}}{FOV}\right), \quad (1)$$

where $n$ is the mode number of the LED radiation pattern, $\phi_{ij}$ is the angle of emergence from the $j$th LED towards the $i$th PD, $A$ is the area of the PD, $d_{ij}$ is the distance between the $j$th LED and the $i$th PD, $\theta_{ij}$ is the angle of incidence at the $i$th PD from the $j$th LED, $FOV$ is the field-of-view of the PD, and $rect(x)$ = 0, for all $|x| > 1$, where $|\cdot|$ represents the absolute value operator or cardinality of a set. The mode number is given by $n = \frac{-\ln(2)}{\ln\cos\Phi_{\frac{1}{2}}}$, where $\Phi_{\frac{1}{2}}$ is the half power semi-angle of the LED.

Assuming perfect channel knowledge and synchronisation at the receiver, the received matrix $\mathbf{Y}$ of order $N_r \times Q$ can be written as

$$\mathbf{Y} = r\mathbf{H}\mathbf{X} + \mathbf{N}, \quad (2)$$

where $r$ is the responsivity of the PD in Amps/Watt and $\mathbf{N}$ is the $N_r \times Q$ noise matrix. Each element in $\mathbf{N}$ is the sum of thermal noise and ambient shot noise which is modelled as i.i.d. Gaussian with zero mean and variance $\sigma^2$. The average SNR is given by $\bar{\gamma} = \frac{r^2}{\sigma^2 N_r} \sum_{i=1}^{N_r} \mathbb{E}[|\mathbf{h}_i\mathbf{X}|^2]$, where $\mathbf{h}_i$ is the $i$th row of $\mathbf{H}$.

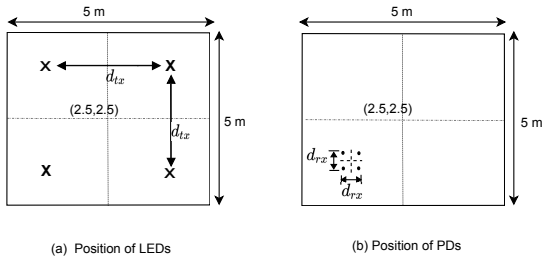


Fig. 2: Placement of the transmitter LEDs and receiver PDs.

The proposed schemes use four transmit LEDs (i.e., $N_t = 4$). These LEDs are placed 0.5 m below the ceiling of the room with $d_{tx}$ as the distance between the LEDs as shown in Fig. 2(a). The placement of the receiver is as shown in Fig 2(b). The coordinate of the receiver location on the receiver plane (which is 0.8 m above the ground) is denoted by $(X_R, Y_R)$. The receiver is assumed to have $N_r = 4$ PDs placed at the corners of a square of side $d_{rx}$ and center $(X_R, Y_R)$. We will vary the location of the receiver in the receiver plane and obtain the spatial distribution of the system performance.

## III. Proposed QCM-OTFS and SM-DCM-OTFS

In this section, we present the proposed QCM-OTFS and SM-DCM-OTFS schemes.

### A. Proposed QCM-OTFS scheme

The block diagram of the proposed QCM-OTFS scheme is shown in Fig. 3. The QCM-OTFS transmitter uses four LEDs. It uses the real and imaginary parts of the complex signal and their signs to convey information through the VLC channel without using Hermitian symmetry. $NM \log_2 |\mathbb{A}|$ information bits are mapped to $NM$ modulation symbols from a modulation alphabet $\mathbb{A}$ (e.g., QAM/PSK), where $|\mathbb{A}|$ is the alphabet size. These information symbols, denoted by $x[k,l]$, $k = 0, 1, \cdots, N-1$, $l = 0, 1, \cdots, M-1$ are populated in a matrix $\mathbf{X}_{in}$ of size $N \times M$ in the delay-Doppler (DD) domain. The matrix $\mathbf{X}_{in}$ is converted into a matrix $\mathbf{X}$ in the time-frequency (TF) domain using $N \times M$-point (2D) inverse symplectic finite Fourier transform (ISFFT) operation. The $(n,m)$th element in $\mathbf{X}$, denoted by $X'[n,m]$, is given by

$$X[n,m] = \frac{1}{MN} \sum_{k=0}^{N-1} \sum_{l=0}^{M-1} x[k,l] e^{j2\pi\left(\frac{nk}{N} - \frac{ml}{M}\right)}, \quad (3)$$

where $n = 0, 1, \cdots, N-1$ and $m = 0, 1, \cdots, M-1$. The TF domain complex matrix $\mathbf{X}$ is converted into a time domain matrix $\bar{\mathbf{S}}$ of size $N \times M$ using $M$-point Heisenberg transform using $M$-point IDFT [15], as

$$\bar{\mathbf{S}} = \sqrt{M} \mathbf{F}_M^H \mathbf{X}^T, \quad (4)$$

where $\mathbf{F}_M^H$ is the $M$-point IDFT matrix given by $\mathbf{F}_M = \left\{\frac{1}{\sqrt{M}} e^{2\pi j \frac{ml}{M}}\right\}_{m,l=0}^{M-1}$. The $(n,m)$th element of $\bar{\mathbf{S}}$, denoted by $\bar{S}[n,m]$, is given by

$$\bar{S}[n,m] = \frac{1}{\sqrt{M}} \sum_{m=0}^{M-1} \mathrm{X}[n,m] e^{j2\pi \frac{ml}{M}}. \quad (5)$$

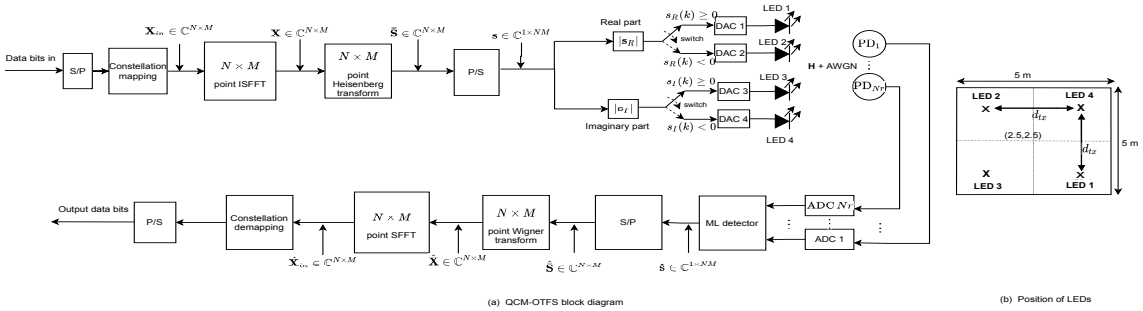


Fig. 3: Proposed QCM-OTFS scheme.

The matrix $\bar{\mathbf{S}}$ is then converted into an $NM$-sized complex vector $\mathbf{s}$ through parallel-to-serial (P/S) conversion. The elements of $\mathbf{s}$ can be written as

$$\mathrm{s}(k) = \mathrm{s}_R(k) + j\mathrm{s}_I(k), \tag{6}$$

where $k = 0, 1, \cdots, NM-1$, and $\mathrm{s}_R$ and $\mathrm{s}_I$ are real and imaginary parts of $s(k)$, respectively. Two LEDs (LED1 and LED2) are used to transmit magnitude of real part of complex number and two different LEDs (LED3, LED4) are used to transmit the imaginary parts as follows:

1) $\mathrm{s}_R^+(k) = |\mathrm{s}_R(k)|$ if $\mathrm{s}_R(k) \geq 0$ and $\mathrm{s}_R^-(k) = |\mathrm{s}_R(k)|$ if $\mathrm{s}_R(k) < 0$,
2) $\mathrm{s}_I^+(k) = |\mathrm{s}_I(k)|$ if $\mathrm{s}_I(k) \geq 0$ and $\mathrm{s}_I^-(k) = |\mathrm{s}_I(k)|$ if $\mathrm{s}_I(k) < 0$.

The vectors $\mathbf{s}_R^+$, $\mathbf{s}_R^-$, $\mathbf{s}_I^+$, and $\mathbf{s}_I^-$ drive LED1, LED2, LED3 and LED4, respectively, and they can be viewed as a $4 \times NM$ transmission matrix $\mathbf{S}$. It can be noted that, because of the above quad-LED transmission strategy, we can drive the LEDs with positive real values without using Hermitian symmetry and DC bias. It is also noted that, in any given channel use, only two LEDs are turned on. We can see that $NM$ symbols from the alphabet $\mathbb{A}$ are sent in $NM$ channel uses in this scheme. Therefore, the achieved rate in bits per channel use (bpcu) is given by $\eta_{\text{qcm-otfs}} = \log_2 |\mathbb{A}|$ bpcu.

Let $\mathbf{Y}$ denote the $N_r \times NM$ received signal matrix corresponding to the transmit signal matrix $\mathbf{S}$. Then, $\mathbf{Y}$ can be written as

$$\mathbf{Y} = r\mathbf{H}\mathbf{S} + \mathbf{W}, \tag{7}$$

where $\mathbf{H}$ is the $N_r \times 4$ MIMO VLC channel matrix, $\mathbf{W}$ is the $N_r \times NM$ noise matrix, and $r$ is the responsivity. Let $\mathbb{S}$ denote the set of all possible QCM-OTFS transmit signal matrices. The maximum likelihood (ML) decision rule can then be written as

$$\hat{\mathbf{S}}_{\text{ML}} = \underset{\mathbf{S} \in \mathbb{S}}{\operatorname{argmin}} \|\mathbf{Y} - r\mathbf{H}\mathbf{S}\|^2. \tag{8}$$

The $\mathbf{s}$ vector corresponding to the detected matrix $\hat{\mathbf{S}}_{\text{ML}}$ is converted into matrix $\hat{\bar{\mathbf{S}}}$ of size $N \times M$ by serial-to-parallel (S/P) conversion. The matrix $\hat{\bar{\mathbf{S}}}$ is converted into TF domain matrix $\hat{\mathbf{X}}$ of size $N \times M$ using Wigner transform as

$$\hat{\mathbf{X}} = \frac{1}{\sqrt{M}} \mathbf{F}_M \hat{\bar{\mathbf{S}}}, \tag{9}$$

where $\mathbf{F}_M$ is the $M$-point DFT matrix. We perform $NM$-point SFFT operation on $\hat{\mathbf{X}}$ to form a matrix $\hat{\mathbf{X}}_{in}$. The $(k,l)$th element of $\mathbf{X}_{out}$ is denoted by $\hat{x}[k,l]$, $k = 0, \cdots, N-1$, $l = 0, \cdots, \frac{M}{2} - 2$, and is given by

$$\hat{x}[k,l] = \sum_{n=0}^{N-1} \sum_{m=0}^{M-1} \hat{\bar{X}}[n,m] e^{-j2\pi\left(\frac{nk}{N} - \frac{ml}{M}\right)}. \tag{10}$$

The $\hat{x}[k,l]$s are mapped to the nearest symbols in $\mathbb{A}$, which are demapped to the corresponding information bits.

### *B. Proposed SM-DCM-OTFS scheme*

The block diagram of the proposed SM-DCM-OTFS scheme is shown in Fig. 4. The SM-DCM-OTFS transmitter consists of two pairs of LEDs. One information bit (index bit) decides which pair among the two will be used to send a given OTFS frame consisting of $NM \log_2 |\mathbb{A}|$ information bits. One LED in the chosen pair transmits the magnitude and the other LED transmits the phase of the complex signal. $NM$ information symbols are populated in a $N \times M$-sized matrix $\mathbf{X}_{in}$ in the DD domain, which is passed through $N \times M$ point ISFFT operation to obtain the signal matrix $\bar{\mathbf{X}}$ in the TF domain. This TF domain signal matrix is converted into the matrix $\bar{\mathbf{S}}$ in the time domain using Heisenberg transform. The matrix $\mathbf{S}$ is converted into a vector $\mathbf{s}$ by P/S conversion. Each element of vector $\mathbf{s}$ is represented in the polar form $s_i = r_i e^{j\phi_i}$, where

$$\begin{aligned} r_i &= |s_i|, \quad r_i \in \mathbb{R}^+ \\ \phi_i &= \arg(s_i), \quad \phi_i \in [0, 2\pi). \end{aligned} \tag{11}$$

Let $\mathbf{r}$ and $\boldsymbol{\phi}$ denote the $NM$-length magnitude and phase vectors corresponding to a given OTFS frame. An index bit $b$ decides which pair of LEDs is used for transmission of a given OTFS frame as follows: 1) if $b = 0$, LED1 and LED2 transmit $\mathbf{r}$ and $\boldsymbol{\phi}$, respectively, and 2) if $b = 1$, LED3 and LED4 transmit $\mathbf{r}$ and $\boldsymbol{\phi}$, respectively. Note that in a given channel use only one pair of LEDs is on and the other pair remains off, forming a $4 \times NM$ transmission matrix $\mathbf{S}$. As can be seen, in this scheme, $NM$ information symbols are conveyed in $NM$ channel uses along with one index bit for each frame. Therefore, the achieved rate in this scheme is given by $\eta_{\text{sm-dcm-otfs}} = \log_2 |\mathbb{A}| + \frac{1}{NM}$ bpcu. At the receiver, inverse operations as shown in Fig. 4 are carried out. After the SFFT operation we look at the non-zero rows of $\hat{\mathbf{X}}_{in}$ to determine $\hat{b}$. After determining $\hat{b}$ and constellation demapping, we recover the information bits.

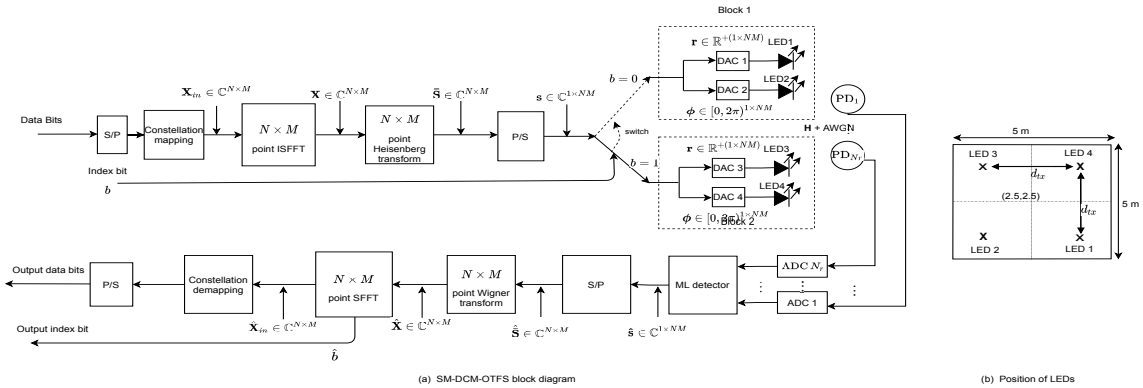


Fig. 4: Proposed SM-DCM-OTFS scheme.

## IV. Performance analysis

In this section, we obtain the upper bound on the BER performance of the proposed schemes and a normalized minimum distance metric to compare the performance of different schemes.

### A. Upper bound on BER

Consider the system model in (7) and the corresponding ML decision rule in (8). Normalizing the elements of the noise matrix to variance one, (7) can be written in the form

$$\mathbf{Y} = \frac{r}{\sigma}\mathbf{HS} + \mathbf{W}. \tag{12}$$

The ML decision rule in (8) can be simplified as

$$\hat{\mathbf{S}}_{ML} = \underset{\mathbf{S}\in\mathbb{S}}{\operatorname{argmin}} \left( \frac{r}{\sigma}\|\mathbf{HS}\|^2 - 2\mathbf{Y}^T\mathbf{HS} \right). \tag{13}$$

Let $\mathbf{S}_1$ and $\mathbf{S}_2$ denote two transmit signal matrices. The pairwise error probability (PEP) of giving a decision in favor of $\mathbf{S}_2$ when $\mathbf{S}_1$ was transmitted can be written as [11]:

$$PEP\left(\mathbf{S}_1 \to \mathbf{S}_2 \mid \mathbf{H}\right) = Q\left(\frac{r}{2\sigma}\left\|\mathbf{H}\left(\mathbf{S}_2 - \mathbf{S}_1\right)\right\|\right). \tag{14}$$

An upper bound on the BER can be obtained using union bound as

$$\begin{aligned} p_e &\leq \frac{1}{|\mathbb{S}|MN}\sum_{i=1}^{|\mathbb{S}|}\sum_{j=1,i\neq j}^{|\mathbb{S}|-1} PEP\left(\mathbf{S}_i \to \mathbf{S}_j \mid \mathbf{H}\right)\frac{d\left(\mathbf{S}_i,\mathbf{S}_j\right)}{\eta} \\ &= \frac{1}{|\mathbb{S}|MN}\sum_{i=1}^{|\mathbb{S}|}\sum_{j=1,i\neq j}^{|\mathbb{S}|-1} Q\left(\frac{r}{2\sigma}\left\|\mathbf{H}\left(\mathbf{S}_j - \mathbf{S}_i\right)\right\|\right)\frac{d\left(\mathbf{S}_i,\mathbf{S}_j\right)}{\eta}, \end{aligned} \tag{15}$$

where $d\left(\mathbf{S}_i,\mathbf{S}_j\right)$ is the Hamming distance between bit mappings corresponding to the signal matrices $\mathbf{S}_i$ and $\mathbf{S}_i$, and $\eta$ is the achieved rate of the system.

### B. Normalized minimum distance of received signal sets

Here, we obtain a metric based on the ratio of the normalized minimum distances of the received signal sets of different schemes in order to compare their performance. We use this metric to assess the relative high-SNR performance of difference schemes. Suppose $\mathbb{S}_{tx} = \{\mathbf{S}_1, \mathbf{S}_2, \cdots, \mathbf{S}_K\}$ is the set of all possible transmit signal matrices of a particular scheme, where $K$ is the size of the signal set. Let $\mathbb{S}_{rx} = \{\mathbf{HS}_1, \mathbf{HS}_2, \cdots, \mathbf{HS}_K\}$ be the corresponding received signal set in the absence of noise for a given $\mathbf{H}$. The matrices in the set $\mathbb{S}_{rx}$ are normalized by the average received signal power to obtain the normalized received signal set $\tilde{\mathbb{S}}_{rx}$ as $\tilde{\mathbb{S}}_{rx} = \{\tilde{\mathbf{Y}}_1, \tilde{\mathbf{Y}}_2, \cdots, \tilde{\mathbf{Y}}_K\}$, where

$$\tilde{\mathbf{Y}}_i = \frac{\mathbf{HS}_i}{\sqrt{\frac{1}{KN_rMN}\sum_{i=1}^{K}\|\mathbf{HS}_i\|^2}}. \tag{16}$$

The minimum distance of the normalized received signal set $\tilde{\mathbb{S}}_{rx}$ can be obtained as

$$d_{\min,\mathbf{H}} = \min_{\tilde{\mathbf{Y}}_i,\tilde{\mathbf{Y}}_j\in\tilde{\mathbb{S}}_{rx},i\neq j}\|\tilde{\mathbf{Y}}_i - \tilde{\mathbf{Y}}_j\|_2. \tag{17}$$

Suppose $\mathbb{S}_{tx_1}$ and $\mathbb{S}_{tx_2}$ are the transmit signal sets of two different schemes. For a given $\mathbf{H}$, let $d^{(1)}_{\min,\mathbf{H}}$ and $d^{(2)}_{\min,\mathbf{H}}$ denote the minimum distances of their corresponding normalized received signal sets. Then, at high SNRs, the BER performance of scheme 1 with signal set $\mathbb{S}_{tx_1}$ will be better than that of scheme 2 with signal set $\mathbb{S}_{tx_2}$, if $d^{(1)}_{\min,\mathbf{H}} > d^{(2)}_{\min,\mathbf{H}}$. The ratio of the minimum distances gives the SNR gap between their BER performance at high SNRs, i.e., the SNR gap in dB is given by

$$\text{SNR}_{\text{gap}} = 20\log\left(d^{(1)}_{\min,\mathbf{H}}/d^{(2)}_{\min,\mathbf{H}}\right). \tag{18}$$

Using the above, we can capture the relative performance of different schemes at different spatial positions of the receiver across the room.

## V. Results and discussions

In this section, we present the analytical and simulation results on the BER performance of the proposed QCM-OTFS and SM-DCM-OTFS in comparison with those of QCM-OFDM and SM-DCM-OFDM. Performance comparison between QCM-OTFS and SM-DCM-OTFS is also made. The simulation parameters used are summarized in Table I.

### A. QCM/SM-DCM OTFS vs QCM/SM-DCM OFDM

Figure 5 shows the simulated BER performance of QCM-OTFS scheme with $M = 2$ delay bins, $N = 4$ Doppler bins, BPSK, and 1 bpcu. The performance of QCM-OFDM with

| | | |
|---|---|---|
| Transmitter | Height from the floor | 3 m |
| | Number of LEDs, $N_t$ | 4 |
| | Elevation | $-90°$ |
| | Azimuth | $0°$ |
| | $\Phi_{1/2}$ | $60°$ |
| | Mode number, $n$ | 1 |
| | $d_{tx}$ | 1 m |
| Receiver | Height from the floor | 0.8 m |
| | Number of PDs, $N_r$ | 4 |
| | Elevation | $90°$ |
| | Azimuth | $0°$ |
| | Responsivity, $r$ | 0.4 Amps/Watt |
| | FOV | $85°$ |
| | $d_{rx}$ | 0.1 m |

TABLE I: System parameters used in the simulations.

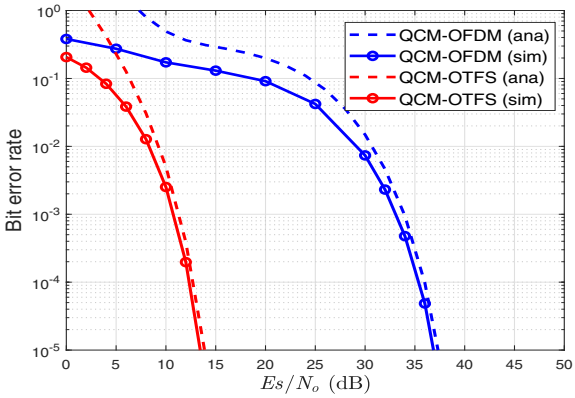


Fig. 5: BER performance of QCM-OTFS ($M = 2$, $N = 4$, BPSK, 1 bpcu) and QCM-OFDM ($M = 8$, BPSK, 1 bpcu) with Rx located at (2,3).

$M = 8$, BPSK, and 1 bpcu is also shown for comparison. The $d_{tx}$ is 1m and the LEDs are placed as shown in Fig. 3. The receiver coordinates are $(X_R, Y_R) = (2, 3)$. For both the OTFS and OFDM based schemes, the corresponding analytical upper bounds on the BER are also plotted. It can be seen that the upper bound is tight at high SNRs. It is also observed that QCM-OTFS outperforms QCM-OFDM by about 22 dB at $10^{-5}$ BER.

Figure 6 shows a similar BER performance comparison between SM-DCM-OTFS (with $M = 2$, $N = 4$, BPSK, 1.125 bpcu) and SM-DCM-OFDM (with $M = 8$, BPSK, 1.125 bpcu). The $d_{tx}$ value is 1m and the LEDs are placed as shown in Fig. 4. The receiver is located at $(X_R, Y_R) = (2, 3)$. Here again, it is observed that the proposed SM-DCM-OTFS outperforms SM-DCM-OFDM by about 4.5 dB at $10^{-5}$ BER.

### *B. Spatial distribution of relative performance*

The BER performance comparisons in Figs. 5 and 6 are done for a fixed receiver location. It is clear that the channel matrix and hence the BER performance vary with receiver location. It is therefore desirable to assess the relative performance of the proposed OTFS based schemes and their OFDM counterparts at different receiver locations across the room. We make this assessment using the normalized minimum distance metric defined in Sec. IV-B. Specifically, we plot the SNR gap between two schemes defined in (18) by placing receiver

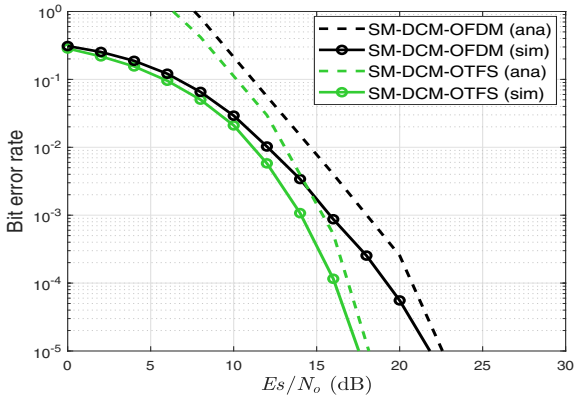


Fig. 6: BER performance of SM-DCM-OTFS ($M = 2$, $N = 4$, BPSK, 1.125 bpcu) and SM-DCM-OFDM ($M = 8$, BPSK, 1.125 bpcu) Rx located at (2,3).

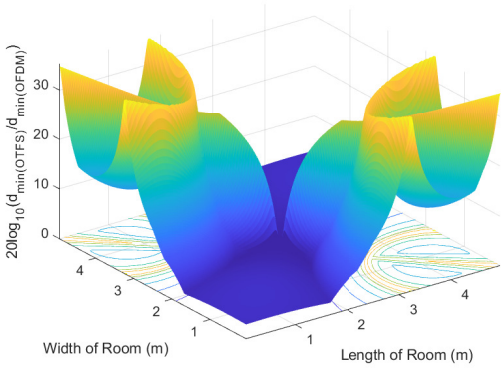


Fig. 7: Spatial distribution of relative normalized $d_{\min}$ of QCM-OTFS with 1 bpcu and QCM-OFDM with 1 bpcu.

at different points at a resolution of 2.5 cm (0.8 m above the ground) across the room. The parameters used in the simulations is given in Table I.

Figure 7 shows the plot of SNR gap (in dB) between QCM-OTFS scheme and QCM-OFDM scheme with 1 bpcu at various locations of the receiver across the room. LEDs are placed as shown in Fig. 3. We observe that the SNR gap between the considered QCM-OTFS and QCM-OFDM schemes is more than 0 dB at all points across the room. This means that QCM-OTFS achieves better performance compared to QCM-OFDM across the room. In certain receiver locations, the SNR gap is observed to be in excess of 30 dB in certain receiver locations.

Figure 8 shows a similar spatial performance comparison between SM-DCM-OTFS and SM-DCM-OFDM, both having 1.125 bpcu rate. The LEDs are placed as shown in Fig. 4. We observe in Fig. 8 that there are both positive and negative values of SNR gap in dB across the room. This means that one scheme can outperform the other depending on the receiver location. A positive dB value of the SNR gap at a receiver location implies that SM-DCM-OTFS performs better in that location, while a negative dB value of the gap implies that SM-DCM-OFDM performs better. In the subfigure in Fig. 8,

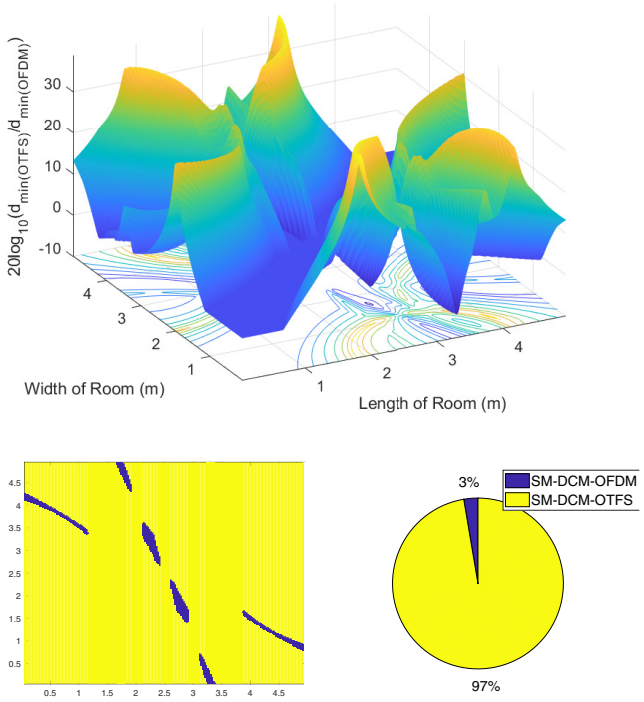


Fig. 8: Spatial distribution of relative normalized $d_{\min}$ of QCM-OTFSand QCM-OFDM with 1.125 bpcu.

the locations with positive and negative dB values are marked as yellow and blue, respectively, which shows the spatial distribution of the relative performance. It is seen that the SM-DCM-OTFS scheme performs better in 97% of the room area.

### C. QCM-OTFS vs SM-DCM-OTFS

Figure 9 shows the BER performance comparison between QCM-OTFS scheme (with $M = 2$, $N = 4$, 4-QAM, 2 bpcu) and SM-DCM-OTFS scheme (with $M = 2$, $N = 4$, 4-QAM, 2.125 bpcu). The receiver location is $(X_R, Y_R) = (2.5, 2.5)$. It can be seen from Fig. 9 that though SM-DCM-OTFS has a higher rate of 2.125 bpcu (compared to 2 bpcu for QCM-OTFS), it achieves better performance compared to QCM-OTFS. This is because the average relative distance between transmit matrices (i.e., $\mathbf{E}[|\mathbf{X}_1 - \mathbf{X}_2|]$ where $\mathbf{X}_1$ and $\mathbf{X}_2$ are two transmit matrices), is higher for SM-DCM-OTFS due to frame indexing.

## VI. Conclusions

We investigated the use of the recently introduced OTFS modulation in indoor multi-LED VLC systems. We proposed two quad-LED schemes, namely, QCM-OTFS and SM-DCM-OTFS schemes, and evaluated their bit error performance through analysis and simulations. Both the schemes do not require Hermitian symmetry or DC bias operations. Our results showed superior performance of the proposed QCM-OTFS and SM-DCM-OTFS schemes compared to those of QCM-OFDM and SM-DCM-OFDM schemes, respectively. The superior performance of OTFS in VLC systems demonstrated in

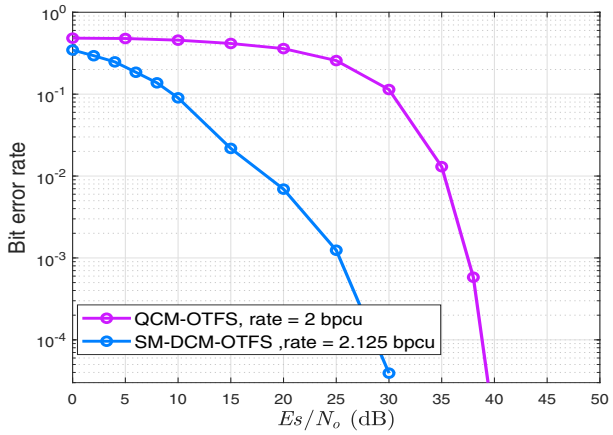


Fig. 9: BER performance of QCM-OTFS ($M = 2$, $N = 4$, 4-QAM, 2 bpcu) and SM-DCM-OTFS ($M = 2$, $N = 4$, 4-QAM, 2.125 bpcu) with at receiver location (2.5,2.5).

this paper can potentially motivate further research on other possible MIMO VLC architectures using OTFS.

## References


[1] P. H. Pathak, X. Feng, P. Hu, and P. Mohapatra, "Visible light communication, networking, and sensing: a survey, potential and challenges," *IEEE Commun. Surveys & Tut.*, vol. 17, no. 4, pp. 2047-2077, 2015.

[2] A. Memedi and F. Dressler, "Vehicular visible light communications: a survey," *IEEE Commun. Surveys & Tut., vol. 23, no. 1, pp. 161-181, 2021.*

*[3] Z. Wang, Q. Wang, W. Huang, and Z. Xu,* Visible Light Communications: Modulation and Signal Processing, Wiley-IEEE Press, 2018.

[4] T. Fath and H. Haas, "Performance comparison of MIMO techniques for optical wireless communications in indoor environments," *IEEE Trans. Commun.*, vol. 61, no. 2, pp. 733-742, Feb. 2013.

[5] S. P. Alaka, T. Lakshmi Narasimhan, and A. Chockalingam, "Generalized spatial modulation in indoor wireless visible light communication", *IEEE GLOBECOM'2015*, Dec. 2015.

[6] O. Gonzlez, R. Prez-Jimnez, S. Rodriguez, J. Rabadn, and A. Ayala, "OFDM over indoor wireless optical channel," *Proc. IEE Optoelectron.*, vol. 152, no. 4, pp. 199-204, Aug. 2005.

[7] J. Armstrong and A. J. Lowery, "Power efficient optical OFDM," *Electron. Lett.*, vol. 42, no. 6, pp. 370-372, Mar. 2006.

[8] N. Fernando, Y. Hong, and E. Viterbo, "Flip-OFDM for optical wireless communications," *IEEE ITW'2011*, pp. 5-9, Oct. 2011.

[9] Y. Li, D. Tsonev, and H. Haas, "Non-DC-biased OFDM with optical spatial modulation," *IEEE PIMRC'2013)*, pp. 486-490, Sep. 2013.

[10] R. Tejaswi, T. L. Narasimhan, and A. Chockalingam, "Quad-LED complex modulation (QCM) for visible light wireless communication," *IEEE WCNC'2016*, pp. 1-6, Apr. 2016.

[11] T. L. Narasimhan, R. Tejaswi, and A. Chockalingam, "Quad-LED and dual-LED complex modulation for visible light communication," available online: arXiv:1510.08805v3 [cs.IT] 24 Jul 2016.

[12] R. Hadani et al., "Orthogonal time frequency space modulation," *IEEE WCNC'2017*, pp. 1-6, Mar. 2017.

[13] R. Hadani et al., "Orthogonal time frequency space modulation," available online: arXiv:1808.00519v1 [cs.IT] 1 August 2018.

[14] K. R. Murali and A. Chockalingam, "On OTFS modulation for high-Doppler fading channels," *ITA'2018*, Feb. 2018.

[15] P. Raviteja, K. T. Phan, Y. Hong, and E. Viterbo, "Interference cancellation and iterative detection for orthogonal time frequency space modulation," *IEEE Trans. Wireless Commun.*, vol. 17, no. 10, pp. 6501-6515, Oct. 2018.

[16] P. Raviteja, E. Viterbo, and Y. Hong, "OTFS performance on static multipath channels," *IEEE Wireless Commun. Lett.*, vol. 8, no. 3, pp. 745-748, Jun. 2019.

[17] J. Zhong, J. Zhou, W. Liu, and J. Qin, "Orthogonal time-frequency multiplexing with 2D Hermitian symmetry for optical-wireless communications," *IEEE Photon. Jl.*, vol. 12, no. 2, pp. 1-10, Apr. 2020.